Theory and Numerical Study of Exciton Dynamics in a Disordered Linear Chain

doi: 10.1063/1.1339267

Theory and numerical study of exciton dynamics in a disordered linear chain

Makoto Shimizu,[a] Shozo Suto, and Takenari Goto
Department of Physics, Graduate School of Science, Tohoku University, Sendai 980-8578, Japan

(Received 5 July 2000; accepted 15 November 2000)

We have formulated the exciton dynamics in a disordered linear chain with exciton wave functions given by the one-dimensional Frenkel exciton Hamiltonian with disorder. It is assumed that exciton–phonon coupling is weak and that the dynamics is governed by the competing processes of phonon scattering and radiative decay. The phonon scattering rate is given on the assumption that excitons do not change the site by the scattering. The strength of exciton–phonon coupling and the density of phonon states are independent of energy. The radiative decay rate is given by the Einstein's A coefficient. The detail of the numerical procedure is also described. Absorption spectra, luminescence spectra, the time response of luminescence intensity, and temperature dependence are calculated for the model system of poly(di-n-hexylsilane) film. It is discussed that long-range dipole–dipole interaction is responsible for the luminescence depolarization. © *2001 American Institute of Physics.* [DOI: 10.1063/1.1339267]

I. INTRODUCTION

Recently, exciton dynamics in luminescent conjugated polymers has been extensively investigated, motivated not only by the application to light emitting devices,[1–4] but also by the physical interests to understand the nature of excited states in conjugated polymers.[5–26] Conjugated polymers are regarded as the ultimate quantum wires because the thickness of polymers is regarded as zero or the atom size. In the one-dimensional system, localization occurs by the Anderson mechanism.[27] This is a comprehensive problem because conformal disorder of polymer chains and the fluctuation of circumstance around polymer strands exist inherently in the polymer systems. Therefore, conjugated polymers provide an ideal stage for the one-dimensional dynamics of excitons affected by disorder.

Among many polymers, poly(di-n-hexylsilane) (PDHS), which is often called a σ-conjugated polymer due to the delocalization of σ-bonding electrons, is a suitable material for the investigation of exciton dynamics using luminescence spectroscopies. The exciton–phonon coupling of PDHS is extremely weak[14] and quantum efficiency for luminescence is quite high.[4] The weak exciton–phonon coupling is important to understand the role of disorder against the translational motion of excitons because strong coupling causes excitons to be self-trapped.[28]

To understand the exciton dynamics in PDHS, the segment model[8–11] has been phenomenologically used. In the segment model, a polymer chain is assumed to be an assembly of segments which are ordered fractions of backbones divided by conformal defects. In analogy with the excitation energy of oligomers,[8,29] it is considered that the longer segment has the lower excitation energy due to the exciton coherence length, i.e., the segment length. The inhomogeneous width of the absorption band is explained by the distribution of the segment length. The Stokes shift is explained in terms of exciton transfer from a shorter excited segment to a longer segment where an exciton recombines. However, the explanation has been always phenomenological. Quantitative inapplicability of the segment model to explain the absorption profile is also pointed out.[14]

The random-walk model[24–26] also describes the exciton dynamics phenomenologically. In this model, an exciton randomly walks within an array (or a box) of the sites of which energies fluctuate in the normal distribution. This model explains the resonant luminescence intensity. However, the model does not give any microscopic picture of the exciton dynamics which is strongly influenced by the phonon scattering rate and the radiative decay rate.

Recently, a quantitative approach has been done with the one-dimensional Frenkel exciton Hamiltonian including disorder.[14] This Hamiltonian was originally used for the linear molecular aggregates[30–34] to understand the absorption spectra.[30,31] This attempt seems to be successful to explain the asymmetric profile of the absorption band seen in low temperature glassy solution of PDHS, although the Hamiltonian was not applied to the exciton dynamics revealed by the luminescent processes. In our previous papers,[5,6] we have reported that the time response of luminescence intensity in PDHS films at 2 K depends on the observed energy. We have also formulated the exciton dynamics as the competing processes of radiative decay and phonon scattering, using exciton wave functions obtained by the one-dimensional Frenkel exciton Hamiltonian with disorder, and have shown that the theory reproduces the time response at 2 K quite well.

In this paper, we report the details of the theory and numerical results for the exciton dynamics in the disordered linear chains. In order to treat the translational coherence of

[a]Present address: The Institute of Physical and Chemical Research (RIKEN), Wako 351-0198, Japan. Electronic mail: shimizoo@postman.riken.go.jp

an exciton obstructed by the conformal disorder, the theory extends the approach by the one-dimensional Frenkel exciton model in the disordered linear chain. Exciton wave functions obtained by the numerical diagonalization of the Hamiltonian are used to formulate the incoherent dynamics of competition between radiative decay and phonon scattering. It is postulated that matrix elements of phonon scattering depend on the spatial overlap between the initial state and the final state of scattering. A numerical procedure is also described. Luminescence spectra and the time response of luminescence intensity as well as temperature dependence are calculated. The importance of long-range dipole–dipole interaction is discussed in comparison with the nearest-neighbor approximation.

II. Theory

A. Basic model

To deal with the exciton dynamics in the disordered linear chain, we adopt the Frenkel exciton Hamiltonian with disorder. The disorder is inherently introduced by conformal disorder in real polymer systems. Neglecting the interaction with the phonon and the photon fields, the exciton Hamiltonian in the site representation is described as

$$H=\sum_{n=1}^{N} E_n|n\rangle\langle n|+\sum_{n\neq m} \beta_{mn}|m\rangle\langle n|. \tag{1}$$

where $\langle n|$ expresses the wave function that the nth site is in the excited state and all the other $N-1$ sites are in the ground states. The on-site excitation energy and the intersite exciton transfer energy originated by the antisymmetrization of wave functions are expressed as E_n and β_{mn}, respectively. To realize disorder, diagonal and off-diagonal disorders are possible. Since disorder in real polymer systems is experimentally unknown, it is practical to examine them separately. In the model material of PDHS, both types of disorder may exist and possibly be correlated. The diagonal disorder occurs when σ-bond length is fluctuated. The off-diagonal disorder occurs mainly when the angle between σ-bonding orbitals is fluctuated. It is shown that both types of disorder can reproduce the absorption spectrum of PDHS in low-temperature glass.[14] We consider that the fluctuation of the rotational angle between the second nearest σ-bonds is the dominant disorder, because these two σ bonds can easily rotate around the σ bond between them. Thus, in this paper, we adopt the off-diagonal disorder and assume the on-site excitation energy to be the uniform magnitude of E_0.

On the assumption that all the transition dipoles have the equal magnitude of μ_0 and that their directions are distributed around the chain direction, the intersite transfer energy β_{mn} is given by the dipole–dipole interaction as

$$\beta_{mn}=\frac{\mu_0^2\{\cos(\theta_m+\theta_n)-3\cos\theta_m\cos\theta_n\}}{|(md+\delta_m)-(nd+\delta_n)|^3} \tag{2}$$

$$\approx\alpha_{mn}|md-nd|^{-3}=\gamma_{mn}|m-n|^{-3}. \tag{3}$$

In Eq. (2), θ_m and δ_m represent the angle and the positional deviations of a transition dipole from the chain axis and from the equilibrium position md, respectively. The mean intersite distance is expressed as d. In Eq. (3), we further introduce the approximation formula for simplification. The angle and the positional disorders are included in the prefactor $\gamma_{mn}\equiv\alpha_{mn}d^{-3}$, which corresponds in magnitude to the intersite transfer energy at the nearest-neighbor distance d. For the prefactor γ_{mn}, the normal distribution with a mean value of γ_0 and a standard deviation of σ is assumed

$$f(\gamma_{mn})=\frac{1}{\sqrt{2\pi}\sigma}\exp\left\{-\frac{(\gamma_{mn}-\gamma_0)^2}{2\sigma^2}\right\}. \tag{4}$$

To investigate the role of the long-range part of the intersite transfer energy β_{mn}, the nearest-neighbor approximation is also examined. In the nearest-neighbor approximation, the intersite transfer is represented as

$$\beta_{mn}=\gamma_{mn}\delta_{m,n\pm1}, \tag{5}$$

where γ_{mn} is given by Eq. (4). When not referred, we assume the full dipole–dipole interaction (3) for the intersite transfer energy.

To obtain exciton wave functions affected by disorder, numerical diagonalization of the Hamiltonian (1) is performed. Obtained time-independent exciton wave functions are expressed in the site representation as

$$|\psi_i\rangle=\sum_{n=1}^{N} a_{in}|n\rangle, \tag{6}$$

where $a_{in}\equiv\langle n|\psi_i\rangle$ represents the exciton amplitude of the ith state at the nth site. The energy of the state is written as ε_i. To estimate the degree of spatial extension of the states, the participation defined as

$$P_i=\left(\sum_{n=1}^{N} a_{in}^4\right)^{-1} \tag{7}$$

is used. The participation represents the localization length or the coherence length of excitons.

B. Exciton dynamics

We formulate the exciton dynamics in the disordered linear chain using the exciton wave functions (6). The following treatment is justified under the condition that an exciton is not polaronic and that the elastic scattering by conformal disorder is faster than the scattering by phonons. There are two cases in phonon scattering. In one case, only the phase of excitons is shifted, and in the other case, excitons are scattered to other states which have different energies. The former elastic scattering contributes to the homogeneous linewidths of exciton states which constitute the inhomogeneously broadened exciton band. However, the theory here only accounts for the latter inelastic scattering because our interest is in the description of exciton relaxation in the inhomogeneously broadened exciton band. Homogeneous linewidth is not accounted for in our theory. The competing processes of phonon scattering between localized exciton states and radiative decay to the ground state are incoherently treated.

The radiative decay rate is given by the Einstein's A coefficient as

$$(\tau_R^{-1})_i=\frac{4\omega_i^3\mu_i^2}{3\hbar c^3}, \tag{8}$$

where $\omega_i\equiv\varepsilon_i/\hbar$ and μ_i represent the transition frequency and the transition dipole moment, respectively. The transition dipole moment is given as

$$\mu_i=\sum_{n=1}^{N}\mu_0 a_{in}\exp(-iknd) \tag{9}$$

$$\approx\sum_{n=1}^{N}\mu_0 a_{in}. \tag{10}$$

The practical expression (10) is derived under the long-wavelength approximation of Eq. (9), where k is the wave number of a photon.

To treat phonon scattering, we abandon the momentum selection rule, because wavenumbers are not good quanta in disordered linear chains. Exciton states are localized by disorder. Thus, we adopt the selection rule in the real space that the spatial overlap between the initial state and the final state determines the matrix element. The matrix element between the ith state and the jth state is given by the square-root of the sum of the products of probabilities a_{in}^2 and a_{jn}^2 to find an exciton at the ith and the jth sites, respectively, as

$$|M_{ij}|^2=\sum_{n=1}^{N}a_{in}^2a_{jn}^2. \tag{11}$$

This formula represents that an exciton does not change the site in phonon scattering. The larger overlap between the states gives the larger matrix element. Using the matrix element (11), the phonon scattering rate from the jth state to the ith state at the temperature T is given by

$$p_{ij}=\begin{cases}c_{tr}|M_{ij}|^2[1+\{\exp(\Delta\varepsilon/k_BT)-1\}^{-1}] & (E_i<E_j),\\ c_{tr}|M_{ij}|^2\{\exp(\Delta\varepsilon/k_BT)-1\}^{-1} & (E_i>E_j),\end{cases} \tag{12}$$

where c_{tr} is the transition constant. The temperature dependence of phonon occupation $\overline{n}$ with the energy $\Delta\varepsilon=|\varepsilon_i-\varepsilon_j|$ is given by the Planck distribution in Eq. (12). The transition constant consists of the density of phonon modes and the constant for exciton–phonon coupling. We postulate that these two factors are independent of energy, despite the extremely small $\Delta\varepsilon$ less than $\Delta\varepsilon_{\min}$. For such small $\Delta\varepsilon$, c_{tr} in Eq. (12) is replaced by $c_{tr}\Delta\varepsilon/\Delta\varepsilon_{\min}$ to prevent divergence of the rate p_{ij} by the Planck distribution at finite temperature. Physically, this postulation corresponds to the uniform density of acoustic phonon modes and the linear coupling between excitons and acoustic phonons in the long-wavelength limit.

C. Numerical procedure

To generate a Hamiltonian (1) for a random chain, the Monte Carlo method is applied in accordance with Eq. (4). Absorption spectra, luminescence spectra, and the time response of luminescence intensity are calculated as an average of the N_{chain} random chains. If not referred, $N_{\text{chain}}=500$ are taken for the average in the results presented below. The number of sites in a chain N is assumed to be 1000.

If we determine the excitation energy E_0 of a site, the mean intersite transfer energy γ_0, and its deviation σ, the Hamiltonians (1) for the N_{chain} chains are determined. Exciton wave functions and their energies are determined by numerical diagonalization of the Hamiltonian (1). Absorption spectra are obtained by

$$A(E)\propto\Sigma_{E-\Delta E/2\leqslant\varepsilon_i<E+\Delta E/2}(\tau_R^{-1})_i$$

$$\propto\sum_{E-\Delta E/2\leqslant\varepsilon_i<E+\Delta E/2}\omega_i^3\left(\sum_{n=1}^{N}a_{in}\right)^2, \tag{13}$$

where the summation is taken for the states of which energies are in the small range of $\pm\Delta E/2$ around E. The second expression gives a spectrum in arbitrary units without determining μ_0. It is assumed that the homogeneous linewidth is within the assumed spectral resolution, ΔE.

Based on the obtained exciton wave functions, the time response and luminescence spectra are sequentially calculated by the small time step of Δt. Let $c_0(t)$ and $c_i(t)$ $(i=1,2,\ldots,N)$ denote the occupation probabilities of the ground state and the ith exciton state at time t. Initial occupations $\mathbf{c}(0)$ caused by the photoexcitation are assumed to be proportional to the radiative decay rate (8) in the excitation bandwidth assumed. The time evolution of the occupation probability $\mathbf{c}(t)$ is sequentially given by

$$\mathbf{c}(t+\Delta t)=D\mathbf{c}(t). \tag{14}$$

The $N+1$ dimensional matrix D which redistributes the occupation probability after the small time Δt is given by

$$D=\begin{pmatrix}D_{11} & (\tau_R^{-1})_1\Delta t & (\tau_R^{-1})_2\Delta t & \cdots & (\tau_R^{-1})_{N-1}\Delta t & (\tau_R^{-1})_N\Delta t\\ 0 & D_{22} & p_{12}\Delta t & p_{13}\Delta t & \cdots & p_{1N}\Delta t\\ 0 & p_{21}\Delta t & \ddots & \ddots & & p_{2N}\Delta t\\ 0 & p_{31}\Delta t & \ddots & \ddots & \ddots & \vdots\\ 0 & \vdots & & \ddots & \ddots & p_{N-1N}\Delta t\\ 0 & p_{N1}\Delta t & p_{N2}\Delta t & \cdots & p_{NN-1}\Delta t & D_{NN}\end{pmatrix}, \tag{15}$$

where the diagonal elements are

$$D_{jj}=1-\sum_{i=1}^{N}{}' D_{ij} \tag{16}$$

to conserve the probability. The prime in the summation indicates that the term with $i=j$ is absent in the sum. $(\tau_R^{-1})_i$ and p_{ij} are given by Eqs. (8) and (12), respectively, if we determine the transition dipole moment μ_0 per site and the transition constant c_{tr}. The time interval Δt should be small enough to satisfy $\Sigma_{i=1}^{N}{}' D_{ij} \ll 1$. The intensity of luminescence from the ith exciton state $(i \neq 0)$ at time t is given by

$$I_i(t)=(\tau_R^{-1})_i c_i(t). \tag{17}$$

To obtain energy-dependent time responses and luminescence spectra, the i-dependent time responses (17) are projected onto the energy space as

$$I_{\mathrm{lumi}}(E,t)=\sum_{E-\Delta E/2 \leqslant \varepsilon_i < E+\Delta E/2} I_i(t). \tag{18}$$

III. RESULTS AND DISCUSSION

Figure 1(a) displays the calculated absorption spectrum. The parameters used are $E_0=5.81$ eV, $\gamma_0=-1.0$ eV, and $\sigma=0.065$ eV, which are optimized for the PDHS film, as reported in Ref. 5. For determining these values, γ_0 is primary estimated from the transition energy of silane-oligomers.[8,29] The absorption bandwidth is determined by σ/γ_0, and the peak energy is shifted by both σ/γ_0 and E_0.

The absorption band in Fig. 1(a) has a peak at 3.38 eV and a width of about 60 meV. The low-energy profile is steep, but the high-energy profile has a long tail due to disorder.[14,30,31] To understand what occurs from the disorder, the density of states, the second power of the transition dipole moment calculated by Eq. (10), and the participation calculated by Eq. (7) are shown as functions of energy in Figs. 1(b), (c), and (d), respectively. The peak of the density of states appears at the band edge as a result of the one-dimensionality, although the peak is broadened by the disorder. The peak locates at 3.40 eV, which is 2 meV higher than the absorption peak.

The second power of the transition dipole moment, μ_i^2, practically gives the oscillator strength because the transition frequency does not significantly vary in this energy range. It has a peak at 3.36 eV, about 2 meV lower than the absorption peak. At energy regions lower than the peak, μ_i^2 becomes smaller at the lower energy. This is because the lower state has a smaller participation, i.e., the lower state is more strongly localized as shown in Fig. 1(d). At energy regions higher than the peak, μ_i^2 steeply decreases with increasing energy. These states have approximately zero oscillator strength if disorder is absent. In the disordered linear chain, the oscillator strength distributes to the higher states because the $k=0$ state and other higher states are mixed by the disorder.

Since the exciton dynamics is assumed to be the competing processes of phonon scattering and radiative decay, μ_0^2/c_{tr} determines the exciton dynamics in arbitrary time scales. In Fig. 2, luminescence spectra for various ratios

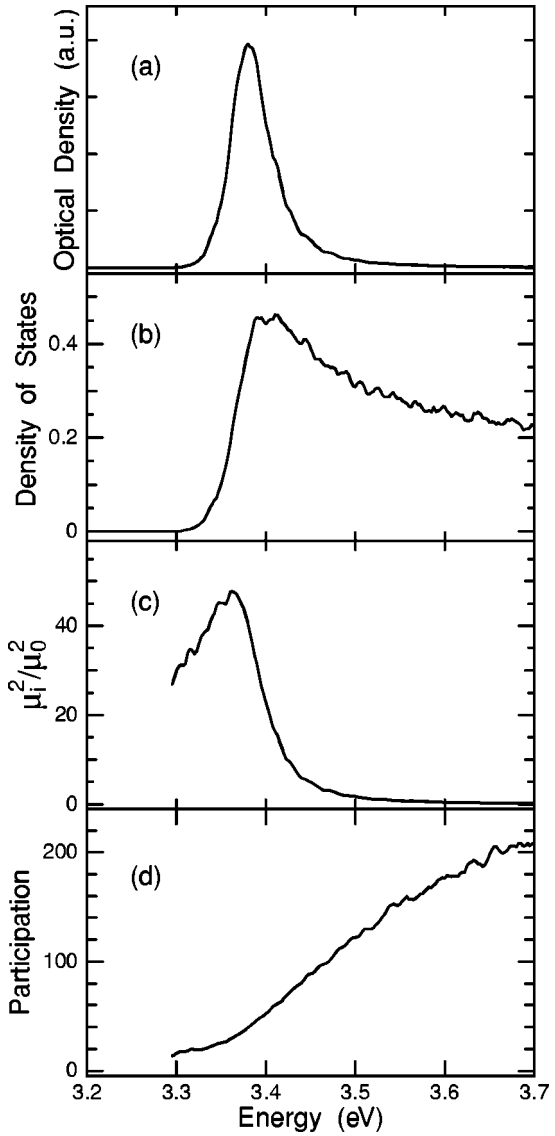

FIG. 1. Energy dependence of absorption (a), the density of states (b), the second power of the transition moment (c), and participation (d) given by the one-dimensional Frenkel exciton Hamiltonian with disorder. In (c), the ordinate is normalized by the second power of the transition moment per monomer unit. Parameters used are $E_0=5.81$ eV, $\gamma_0=-1.0$ eV, and $\sigma=0.065$ eV.

μ_0^2/c_{tr} are shown with solid lines. Ratios μ_0^2/c_{tr} in (a) and (c) are one-tenth and ten times as large as that in (b), respectively. To determine the absolute time scale, $\mu_0=1.7\times10^{-18}$ esu cm and $c_{tr}=6.0\times10^{12}$ s^{-1} for (a), $\mu_0=3.0\times10^{-18}$ esu cm and $c_{tr}=1.9\times10^{12}$ s^{-1} for (b), and $\mu_0=5.3\times10^{-18}$ esu cm and $c_{tr}=6.0\times10^{11}$ s^{-1} for (c), respectively, are used. The values for (b) are the optimized values according to the time response, as described below. Temperature is assumed to be 0 K. The dotted line in (b) is the absorption spectrum for comparison. The Stokes shift, i.e., the difference in energy between absorption and luminescence, is small and only decreases slightly with increasing μ_0^2/c_{tr} in the realistic range of two orders from (a) to (c). Spectral widths are nearly independent of μ_0^2/c_{tr}, and it is actually impossible to fit the experimental data. The numerical result has twice the width as large as the experimental

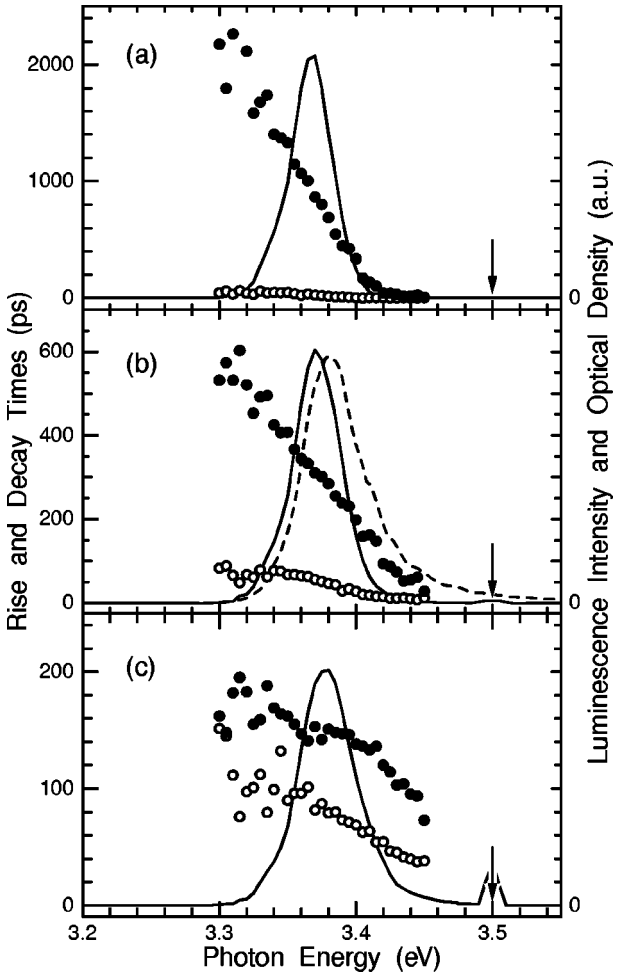

FIG. 2. Luminescence spectra (solid lines) and the energy dependence of rise times (open circles) and decay times (closed circles) of luminescence intensity at $T=0$. Arrows indicate the excitation energies. A dotted line in (b) shows the absorption spectrum [same as Fig. 1 (a)] for comparison. Parameters used are $\mu_0=\mu_0^{\text{opt.}}\times 10^{-1/4}$ and $c_{tr}=c_{tr}^{\text{opt.}}\times 10^{1/2}$ for (a), $\mu_0=\mu_0^{\text{opt.}}=3.0\times 10^{-18}$ esu cm and $c_{tr}=c_{tr}^{\text{opt.}}=1.9\times 10^{12}$ s^{-1} for (b), and $\mu_0=\mu_0^{\text{opt.}}\times 10^{1/4}$ and $c_{tr}=c_{tr}^{\text{opt.}}\times 10^{-1/2}$ for (c). $x^{\text{opt.}}$ means the optimized value of x.

result. Two reasons are possible causes of this deviation in the spectral width. One is the error in determining the parameters of model Hamiltonian (1), because a spectral width of luminescence primarily depends on the distribution of states which have oscillator strength. The other possible reason is the deviation of the real system from the ideal one-dimensionality due to the interchain interaction. In real PDHS films, small exciton transfer to neighboring polymer chains may be possible. But, the interaction should be small because the interchain distance is large due to the long side groups in PDHS.

Figure 3 shows time response at 3.33, 3.36, 3.39, and 3.41 eV with the parameters for Fig. 2(b). As displayed, each response has a rise time which is larger at lower energies. Decay is faster at higher energies. The decay profiles are nearly exponential, although appreciably deviate at higher energies, as at 3.41 eV. This deviation occurs because a time response at an energy is the statistical superposition of the time responses of a number of states which have different

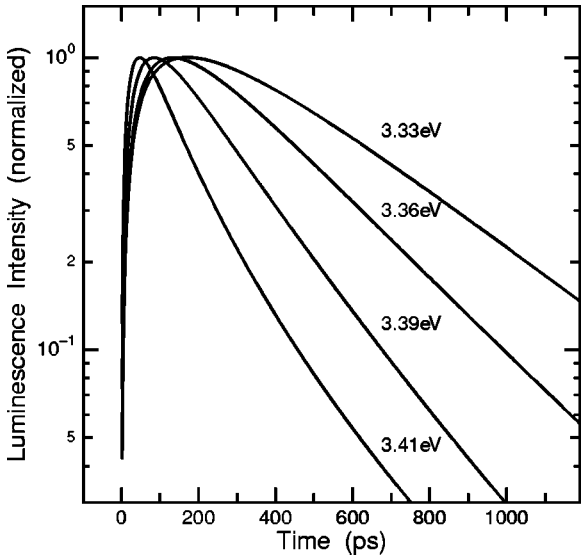

FIG. 3. Time responses of luminescence intensity at 3.33, 3.36, 3.39, and 3.41 eV. Parameters used are the same as those used for Fig. 2(b).

decay rates. So, the deviation at the higher energy means that the distribution of decay rate of states is larger at the higher energy.

Although not exactly exponential, we determined rise times τ_{rise} and decay times τ_{dec} of numerically calculated time responses, in order to discuss the time responses quantitatively. The numerical results are least-square fit to the phenomenological formula,

$$I_{\text{lumi}}(E,t)\propto -\exp(-t/\tau_{\text{rise}})+\exp(-t/\tau_{\text{dec}}). \tag{19}$$

In this way, rise times and decay times are determined for various parameters and shown in Figs. 2(a)–(c) with open and closed circles, respectively. In any parameters, both rise times and decay times are larger at the lower energies, but the ratio of a rise time to a decay time is larger for the larger ratio of μ_0^2 to c_{tr}.

Since the time scale is arbitrarily determined by the absolute magnitude of c_{tr} and μ_0 in the theory, the ratio of the rise time to the decay time, rather than the absolute values of the rise and the decay times, is the important manifestation of the exciton dynamics. Therefore, the optimized parameters in Fig. 2(b) are determined so that the ratio of the rise time to the decay time at the peak energy in the numerical result is the same as that in the experimental result at 2 K.[5] In contrast to spectral widths and Stokes shifts, time responses are quite sensitive to the ratio, μ_0^2/c_{tr}. When we take μ_0^2/c_{tr} one-tenth as small as that in Fig. 2(b), the ratio of the rise time to the decay time becomes one-thirtieth, as shown in (a). When μ_0^2/c_{tr} is ten times as large as that in (b), the ratio is about one half, as shown in (c). Finally, after determining the ratio, absolute values are determined to fit the real time scale. With these optimized parameters, the distributions of rise times and decay times agree with the experimental result in which both times are larger at the lower energy, very well if the distributions are normalized by the energy deviation form the peak energy.

To understand the elementary processes of the exciton dynamics, an example of the wave functions for the lowest

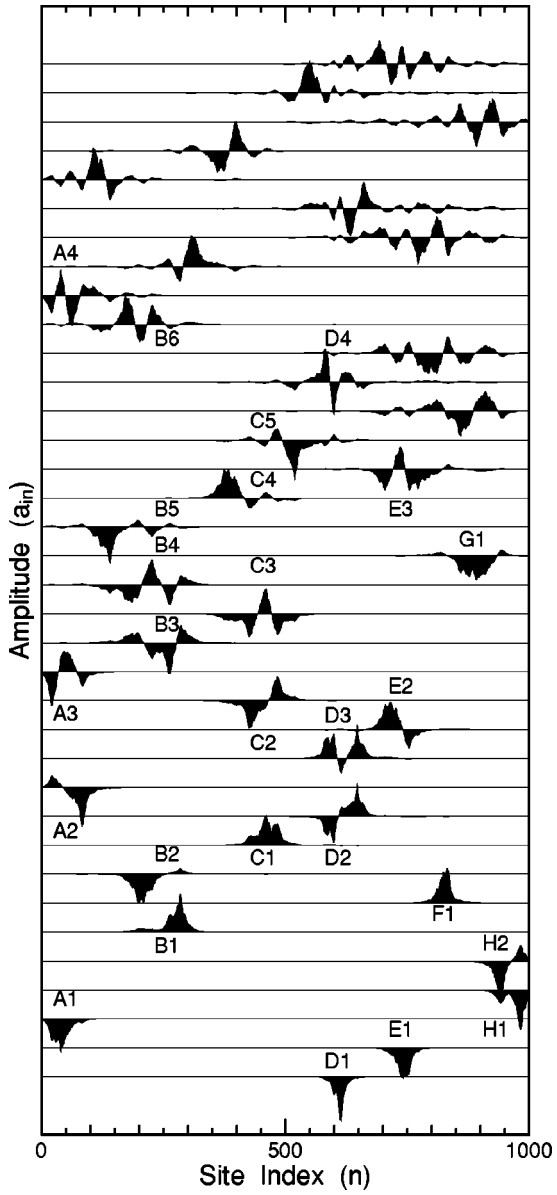

FIG. 4. An example of wave functions of the lowest 36 exciton states generated in a disordered linear chain including the long-range dipole–dipole interaction (3). The amplitude a_{in} is plotted against the site n. The higher-energy state is displayed at the higher position. Characters (A)–(H) and numbers (1)–(6) represent the hidden structures and the quantum numbers of the states within a hidden structure, respectively.

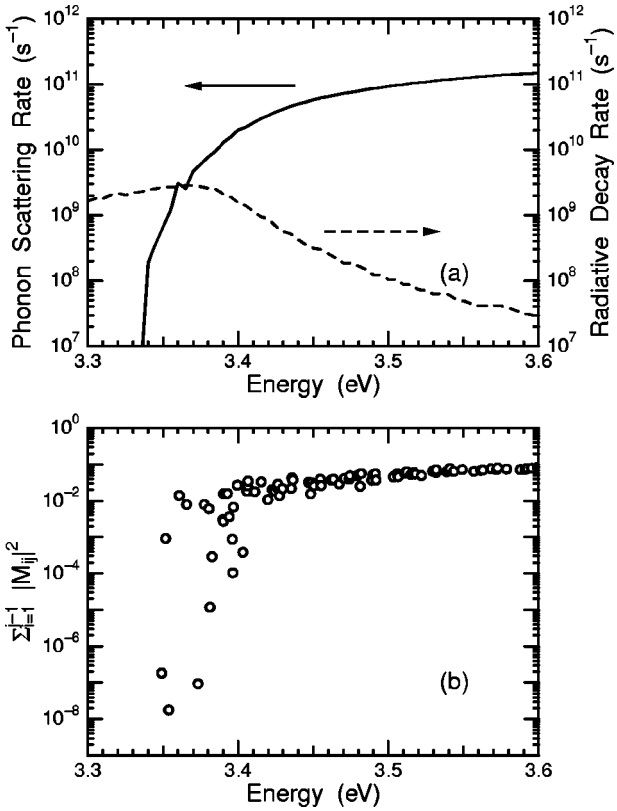

FIG. 5. (a) Energy dependence of the expectation values of the phonon scattering rate (a solid line) and the radiative decay rate (a dotted line). Five hundred random chains are taken for the average. (b) The distribution of $\Sigma_{i=1}^{j-1'}|M_{ij}|^2$ for the states generated in a chain.

36 exciton states generated in a random chain is shown in Fig. 4. The wave functions are presented from the bottom in the order of energy in the site representation. Parameters used are the same as those used in Fig. 1. The energies of these states are 3.33 to 3.44 eV, which are in the energy range of the absorption band. As shown in Fig. 1(d), a lower state tends to be more strongly localized.

Lowest states are predominantly localized in some small segments of the chain. It is possible to identify the ground and excited states localized in the same segment. This localized energy structure is called a hidden structure.[35,36] Characters (A)–(H) and numbers (1)–(6) in the figure represent the identification of the hidden structure and the quantum number within a hidden structure, respectively. The hidden structure is intuitively acceptable if we pay attention to the number of nodes of wave functions. We note, however, that the existence of the hidden structure is not mathematically proven. The hidden structure is interesting because it relates the microscopic description of the exciton dynamics in the continuously disordered chain to the description by the phenomenological segment model. In the segment model, conformal defects are postulated as barriers which divide segments. On the other hand, the hidden structures, which are analogs of the segments in the phenomenological segment model, are generated by the interference of wave functions reflected by continuous disorder.

Figure 5(a) displays the energy dependence of the expectation values of the phonon scattering rate at $T=0$ and the radiative decay rate by solid and dashed lines, respectively. Assumed parameters are the same as those for Fig. 2(b). The radiative decay rate has a peak at 3.7 eV as predicted by the transition dipole moment shown in Fig. 1(c). The phonon scattering rate becomes dramatically small at the lower energy. This is because, at low temperature, it is possible for an exciton to be scattered only to the lower-energy states as described in Eq. (12) and the lower-energy states have the smaller number of possible final states for the phonon scattering. Moreover, due to the stronger localization at the lower energy as shown in Fig. 1(d) and Fig. 4, matrix elements (11) between the low-energy states are small. At 3.36 eV, the rates for the phonon scattering and for the radiative decay become nearly equal. This energy is smaller than the

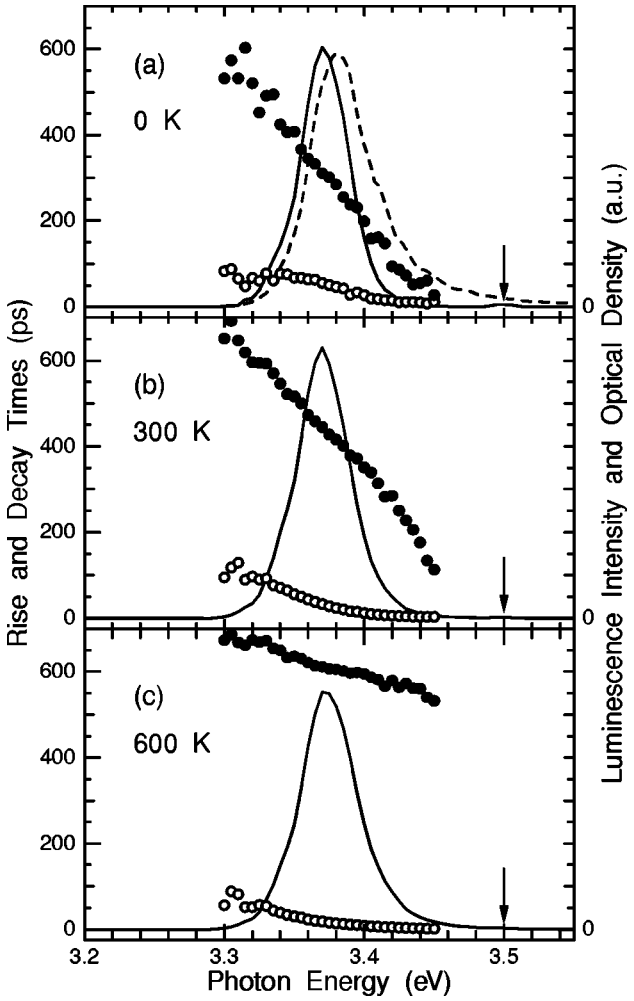

FIG. 6. Temperature dependence of luminescence spectra and the time response of luminescence intensity. Solid lines, open and closed circles, and arrows show luminescence spectra, rise and decay times, and excitation energies, respectively. Assumed temperatures are 0 K for (a), 300 K for (b), and 600 K for (c). A dotted line in (a) shows the absorption spectrum [same as Fig. 1(a)] for comparison.

luminescence peak energy in Fig. 2(b) by 10 meV. This difference is attributed to the large distribution of the phonon scattering rate. Figure 5(b) shows the distribution of

$$\sum_{i=1}^{j-1}{}' |M_{ij}|^2$$

for the states in a chain. This sum of matrix elements to the lower states gives the phonon scattering rate (12) at $T=0$. Since the distribution of the phonon scattering rate is quite large in the range less than 3.4 eV, the mean value is dominated by the states which possess large scattering rates. However, the contribution of these states to luminescence is small because excitons are scattered from these states before they emit photons.

To clarify the exciton dynamics governed by phonon scattering, temperature dependence is important because the phonon scattering rate is a function of temperature. In Fig. 6, the temperature dependence of luminescence spectra, rise times, and decay times are shown by solid lines, open circles, and closed circles, respectively. A dotted line in (a) shows the absorption spectrum for comparison. The excitation energy is assumed to be 3.5 eV and is shown by arrows. The rise and the decay times are determined by the same procedure as those for Fig. 2. All the parameters despite temperature T are the same as those used in Figs. 1 and 2(b). In Fig. 6, (a), (b), and (c) show the results for the temperatures of zero [same as Fig. 2(b)], 300, and 600 K, respectively. The absorption spectrum is independent of temperature in our model. With increasing temperature, the peak does not shift, but the high-energy tail of the band becomes slightly larger. This is due to the thermal distribution of excitons at high temperature. In terms of the time response, the rise time becomes small, and the decay time increases and becomes less dependent on energy at higher temperature. The small rise time is brought by the increased phonon occupation which increases the phonon scattering rate (12). The distribution of decay times is interpreted as that, at high temperature, excitons form a quasithermal distribution and the net rate of energy relaxation is small. Thus, the contribution of the phonon scattering to the decay time is less dominant. This temperature dependence predicted by our theory qualitatively agrees with the experimental results in the PDHS film.[37]

In spite of the qualitative success in the temperature dependence, we have to note the limit of our approach in which the contribution of the homogeneous linewidth to the whole spectra is neglected. According to our numerical results, the total rate of inelastic phonon scattering and radiative decay is less than 1×10^{11} s^{-1} for the states in the energy range of luminescence spectra, even at 600 K. Therefore, our treatment is self-consistent. In reality, however, there is a possibility that the homogeneous linewidth broadened by elastic phonon scattering contributes significantly to the spectra. At low temperatures, homogeneous linewidths were measured by the spectral hole-burning technique for PDHS in glass. The linewidths were 0.2 meV at 2 K and 0.8 meV at 30 K,[14] which are small enough to justify our treatment. At higher temperature, one can expect the homogeneous linewidth to be far broadened. Experimentally, the homogeneous linewidth has not been clarified at high temperature up to now.

We have taken the full dipole–dipole interaction (3) into account in the results presented above. On the other hand, it is found that the absorption spectrum, the luminescence spectrum, and the rise and the decay times can be reproduced with the nearest-neighbor approximation (5) as well as with the full interaction (3). In our previous paper,[5] we reported that it is impossible to reproduce the time response with the nearest-neighbor approximation, but this impossibility has been found a fault due to a numerical error. Other numerical results in our previous paper, for example, wave functions and the participation in the nearest-neighbor approximation are correct. In the nearest-neighbor approximation, the same experimental results are reproduced by $E_0=5.8$ eV, $\gamma_0=-1.2$ eV, $\sigma=0.05$ eV, $\mu_0=4.2\times10^{-18}$ esu cm, and $c_{tr}=9.4\times10^{11}$ s^{-1}. The reason for taking γ_0 as -1.2 eV is to make the sum of all the excitation transfer energies $\Sigma_{n\neq m}\beta_{mn}$ equal to that with the full interaction (3).

Figure 7 shows an example of the lowest 36 states generated by the Hamiltonian (1) with the nearest-neighbor approximation (5), for comparison with those in Fig. 4 with the

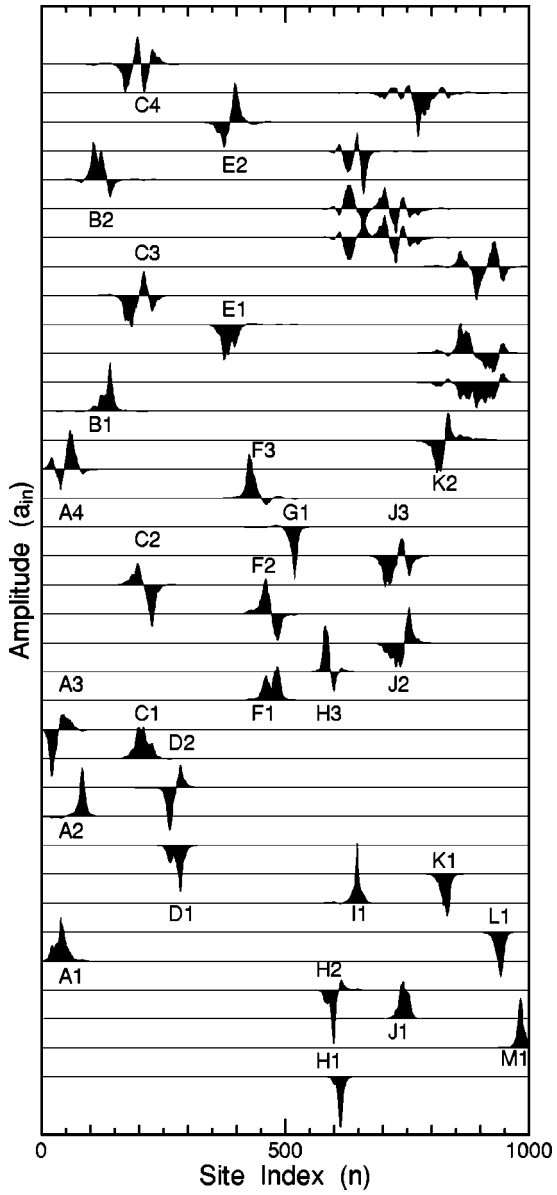

FIG. 7. An example of wave functions of the lowest 36 exciton states generated in a disordered linear chain in the nearest-neighbor approximation (5). The amplitude a_{in} is plotted against the site n. The higher-energy state is displayed at the higher position. Characters (A)–(M) and numbers (1)–(4) represent the hidden structures and the quantum numbers of the states within a hidden structure, respectively.

full interaction (3). The wave functions in the nearest-neighbor approximation are more strongly localized and the hidden structures are seen more clearly than those with the full interaction (3). Classification of the states to 14 hidden structures is shown in the same manner as in Fig. 4. Overlap between two states which belong to different hidden structures is extremely small.

The different nature between the exciton dynamics with the full interaction (3) and that in the nearest-neighbor approximation (5) is clearly seen in the matrix elements (11) of phonon scattering. We have taken $\langle |M_{ij}^2| \rangle$, the mean values of the square of matrix elements between the states which belong to the same and the different hidden structures, following the assignment of the states to hidden structures shown in Figs. 4 and 7, although the assignment is not necessarily definitive. With the full interaction, the mean values are 7×10^{-3} within the same hidden structure and 2×10^{-4} between the neighboring hidden structures. In the nearest-neighbor approximation, the mean values are 1×10^{-2} within the same hidden structure and 2×10^{-5} between the neighboring hidden structures. Therefore, with the full interaction, an exciton can be scattered to the states of neighboring hidden structures and causes large spatial migration along a polymer chain. In contrast, in the nearest-neighbor approximation, an exciton cannot be scattered to the states of neighboring hidden structures within their lifetimes.

In PDHS solution at room temperature and in glassy solution at low temperature, it is reported that luminescence depolarization occurs in the time range of a few hundred picoseconds.[8–11] Considering that the transition dipole of an exciton in PDHS is along a polymer chain, spatial migration of excitons by phonon scattering is necessary to bring out the luminescence depolarization. Therefore, the appropriate description of the exciton dynamics must include the long-range dipole–dipole interaction (3). This interaction is responsible for the exciton migration and the luminescence depolarization.

IV. SUMMARY

We have reported the theory of the exciton dynamics in the disordered linear chains. It is assumed that exciton–phonon coupling is weak and that the dynamics is governed by the competing processes of phonon scattering and radiative decay. The one-dimensional Frenkel exciton Hamiltonian with disorder is used to provide exciton wave functions. The radiative decay rate is given by the Einstein's A coefficient with the long-wavelength approximation. The phonon scattering rate is given on the assumption that an exciton does not change the site in the scattering and that the exciton–phonon coupling and the density of phonon modes are independent of energy. A numerical procedure to obtain absorption spectra, luminescence spectra, and the time response of luminescence intensity, as well as temperature dependence is also presented. Calculation is performed for the PDHS film and the result reproduces the luminescence time response quite well. It is discussed that the long-range dipole–dipole interaction is responsible for the luminescence depolarization.

ACKNOWLEDGMENTS

The authors thank Professor Yosuke Kayanuma of Osaka City University, Professor Komajiro Niizeki of Tohoku University, and Dr. Tsuyoshi Kato of Electrotechnical Laboratory for their useful discussions.

[1] R. H. Friend, R. W. Gymer, A. B. Holmes, J. H. Burroughes, R. N. Marks, C. Taliani, D. D. C. Bradley, D. A. Dos Santos, J. L. Bredas, M. Logdlund, and W. R. Salaneck, Nature (London) **397**, 121 (1999).
[2] Y. Cao, I. D. Parker, G. Yu, C. Zhang, and A. J. Heeger, Nature (London) **397**, 414 (1999).
[3] C. W. Tang and S. Slyke, Appl. Phys. Lett. **51**, 913 (1987).
[4] N. Kamata, S. Aihara, W. Ishizaka, M. Umeda, D. Terunuma, K. Yamada, and S. Furukawa, J. Non-Cryst. Solids **227-230**, 538 (1998).

[5] M. Shimizu, S. Suto, T. Goto, A. Watanabe, and M. Matsuda, Phys. Rev. B **58**, 5032 (1998).
[6] S. Suto, M. Shimizu, T. Goto, A. Watanabe, and M. Matsuda, J. Lumin. **76–77**, 486 (1998).
[7] S. Suto, M. Shimizu, T. Goto, A. Watanabe, and M. Matsuda, Jpn. J. Appl. Phys., Suppl. **34-1**, 185 (1994).
[8] K. A. Klingensmith, J. W. Downing, R. D. Miller, and J. Michl, J. Am. Chem. Soc. **108**, 7438 (1986).
[9] Y. R. Kim, M. Lee, J. R. G. Thorne, and R. M. Hochstrasser, Chem. Phys. Lett. **145**, 75 (1988).
[10] J. R. G. Thorne, R. M. Hochstrasser, and J. M. Zeigler, J. Phys. Chem. **92**, 4275 (1988).
[11] J. R. G. Thorne, A. Tilgner, Y. R. Kim, J. M. Zeigler, H. P. Trommsdorff, and R. M. Hochstrasser, J. Lumin. **53**, 170 (1992).
[12] A. Elschner, R. F. Mart, L. Pautmeier, H. Bassler, M. Stolka, and K. McGrane, Chem. Phys. **150**, 81 (1991).
[13] R. D. Kepler and Z. G. Soos, Phys. Rev. B **47**, 9253 (1993).
[14] A. Tilgner, H. P. Trommsdorf, J. M. Zeigler, and R. M. Hochstrasser, J. Chem. Phys. **96**, 781 (1992).
[15] U. Rauscher, H. Bassler, D. D. C. Bradley, and M. Hennecke, Phys. Rev. B **42**, 9830 (1990).
[16] U. Rauscher, L. Schutz, A. Greiner, and H. Bassler, J. Phys.: Condens. Matter **1**, 9751 (1989).
[17] U. Lemmer, R. F. Mahrt, Y. Wada, A. Greiner, H. Bassler, and E. O. Gobel, Chem. Phys. Lett. **209**, 243 (1993).
[18] S. Heun, R. F. Mahrt, A. Greiner, U. Lemmer, H. Bassler, D. A. Halliday, D. D. C. Bradley, P. L. Burn, and A. B. Holmes, J. Phys.: Condens. Matter **5**, 247 (1993).
[19] C. M. Heller, I. H. Campbell, B. K. Laurich, D. L. Smith, D. D. C. Bradley, P. L. Burn, J. P. Ferraris, and K. Mullen, Phys. Rev. B **54**, 5516 (1996).
[20] L. Pautmeier, U. Rauscher, and H. Bassler, Chem. Phys. **146**, 291 (1990).
[21] U. Rauscher, H. Bassler, and R. Taylor, Chem. Phys. Lett. **162**, 127 (1989).
[22] U. Rauscher and H. Bassler, Macromolecules **23**, 398 (1990).
[23] A. Watanabe, T. Kodaira, and O. Ito, Chem. Phys. Lett. **273**, 227 (1997).
[24] G. Schonherr, H. Bassler, and M. Silver, Philos. Mag. B **44**, 47 (1981).
[25] L. Pautmeier, R. Richert, and H. Bassler, Philos. Mag. Lett. **59**, 325 (1989).
[26] B. Mollay, U. Lemmer, R. Kersting, R. F. Mahrt, H. Kurz, H. F. Kauffmann, and H. Bassler, Phys. Rev. B **50**, 10769 (1994).
[27] P. W. Anderson, Phys. Rev. **109**, 1492 (1958).
[28] T. Kobayashi, in *Relaxation in Polymers*, edited by T. Kobayashi (World Scientific, Singapore, 1993), p.1.
[29] H. Kishida, H. Tachibana, K. Sakurai, M. Matsumoto, S. Abe, and Y. Tokura, J. Phys. Soc. Jpn. **65**, 1578 (1996).
[30] J. Klafter and J. Jortner, J. Chem. Phys. **68**, 1513 (1978).
[31] H. Fidder, J. Knoester, and D. A. Wiersma, J. Chem. Phys. **95**, 7880 (1991).
[32] E. W. Knapp, Chem. Phys. **85**, 73 (1984).
[33] H. Fidder, J. Terpstra, and D. A. Wiersma, J. Chem. Phys. **94**, 6895 (1991).
[34] R. Gadonas, K.-H. Feller, A. Pugzlys, G. Jonusauskas, J. Oberle, and C. Rulliere, J. Chem. Phys. **106**, 8374 (1997).
[35] V. A. Malyshev, J. Lumin. **55**, 225 (1993).
[36] V. A. Malyshev and P. Moreno, Phys. Rev. B **51**, 14587 (1995).
[37] M. Shimizu, S. Suto, T. Goto, A. Watanabe, and M. Matsuda, Phys. Rev. B (in press).